JACS
JOURNAL OF THE AMERICAN CHEMICAL SOCIETY
Article
Cite This: J. Am. Chem. Soc. 2018, 140, 7681−7687
pubs.acs.org/JACS

Direct Conversion of Methane to Methanol on Ni-Ceria Surfaces: Metal−Support Interactions and Water-Enabled Catalytic Conversion by Site Blocking

Pablo G. Lustemberg,[†] Robert M. Palomino,[‡] Ramón A. Gutiérrez,[§] David C. Grinter,[∥] Mykhailo Vorokhta,[⊥] Zongyuan Liu,[‡] Pedro J. Ramírez,[§] Vladimír Matolín,[⊥] M. Verónica Ganduglia-Pirovano,*[,#] Sanjaya D. Senanayake,*[,‡] and José A. Rodriguez*[,‡]

[†]Instituto de Fisica Rosario (IFIR), CONICET-UNR, , Bv. 27 de Febrero 210bis, S2000EZP Rosario, Santa Fe, Argentina
[‡]Chemistry Department, Brookhaven National Laboratory, Upton, New York 11973, United States
[§]Facultad de Ciencias, Universidad Central de Venezuela, Caracas 1020-A, Venezuela
[∥]Surfaces and Interfaces, Diamond Light Source, Harwell Science and Innovation Campus, Didcot, Oxfordshire OX11 0DE, United Kingdom
[⊥]Department of Surface and Plasma Science, Faculty of Mathematics and Physics, Charles University, Prague, Czech Republic
[#]Instituto de Catálisis y Petroleoquímica, CSIC, C/Marie Curie 2, 28049 Madrid, Spain

Supporting Information

ABSTRACT: The transformation of methane into methanol or higher alcohols at moderate temperature and pressure conditions is of great environmental interest and remains a challenge despite many efforts. Extended surfaces of metallic nickel are inactive for a direct $CH_4 \rightarrow CH_3OH$ conversion. This experimental and computational study provides clear evidence that low Ni loadings on a $CeO_2(111)$ support can perform a direct catalytic cycle for the generation of methanol at low temperature using oxygen and water as reactants, with a higher selectivity than ever reported for ceria-based catalysts. On the basis of ambient pressure X-ray photoemission spectroscopy and density functional theory calculations, we demonstrate that water plays a crucial role in blocking catalyst sites where methyl species could fully decompose, an essential factor for diminishing the production of CO and CO_2, and in generating sites on which methoxy species and ultimately methanol can form. In addition to water-site blocking, one needs the effects of metal−support interactions to bind and activate methane and water. These findings should be considered when designing metal/oxide catalysts for converting methane to value-added chemicals and fuels.

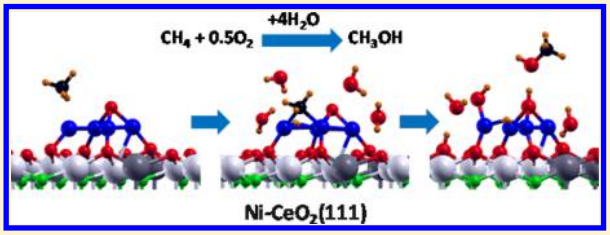

INTRODUCTION

Besides being an excellent source of energy, natural gas is a cheap and abundant source of carbon for the chemical industry. Methane is the primary component of natural gas and a potent greenhouse gas, but it is difficult to convert it to upgraded fuels or chemicals due to the strength of the C−H bonds in the molecule (104 kcal/mol).[1] A synthetic path for a direct $CH_4 \rightarrow CH_3OH$ transformation is a major goal in the industrial use of methane since the alcohol is useful as a fuel and a good building block for the generation of many chemical goods.[1] The reaction of molecular oxygen with methane can follow two different reaction paths:[2]

$$CH_4 + \frac{1}{2}O_2 \rightarrow CH_3OH \quad (1)$$

$$CH_4 + \frac{1}{2}O_2 \rightarrow CO + 2H_2 \quad (2)$$

From a thermodynamic viewpoint, both reaction paths are exothermic, but at temperatures higher than 600 K, path 2 is more favorable.[2] Thus, to generate CH_3OH as a stable product or intermediate, one must find catalytic materials which can bind and activate CH_4 at temperatures below 500 K.[2−6]

In recent years, the direct catalytic conversion of methane to methanol has sparked considerable interest.[3−15] The direct conversion is performed by the enzyme methane monooxygenase, but it is very difficult to use this biological system for major industrial-scale processes.[7,10] A core of three copper ions is probably responsible for the $CH_4 \rightarrow CH_3OH$ transformation in the enzyme.[4] Copper-exchanged zeolites are able to mimic the activity of the methane monooxygenase.[3−6,12] Inside the structure of zeolites, CH_3OH can be generated by sequential dosing of O_2 and CH_4, and at the end the alcohol is flushed out with H_2O.[3−6] A catalytic $CH_4 \rightarrow CH_3OH$ conversion is also possible inside copper-exchanged zeolites[12] or on a model inverse oxide/metal catalyst such as $CeO_2/CuO_x/Cu(111)$.[14] In this study, we focus our attention on the performance of a

Received: April 9, 2018
Published: May 28, 2018

DOI: 10.1021/jacs.8b03809
J. Am. Chem. Soc. 2018, 140, 7681−7687

catalyst with a conventional Ni/CeO_2 configuration that can be used in technical applications. Using a combination of experiment (ambient pressure X-ray photoelectron spectroscopy) and theory (density functional calculations), we show that a low-loaded $Ni/CeO_2(111)$ system activates CH_4 at 300 K and then, with the help of water, which prevents sequential cleavage of C−H bonds, performs a direct catalytic cycle for the generation of CH_3OH at relatively low temperatures (450 K). These results show the impact that metal−support interactions have on C−H and O−H bond breaking and the beneficial effect of water to diminish the production of CO and CO_2 during methane conversion to methanol. The mechanisms and outcomes demonstrated here are valid also for the production of other alcohols.

METHODS

Experimental Methods. The experiments examining the conversion of methane into methanol over $Ni/CeO_2(111)$ surfaces were performed in an apparatus which contains an ultrahigh vacuum (UHV) chamber for surface characterization and a batch microreactor for catalytic studies.[16−18] The UHV chamber was set up with X-ray photoelectron spectroscopy (XPS), Auger electron spectroscopy (AES), ion-scattering spectroscopy (ISS), low-energy electron diffraction (LEED), and temperature-programmed desorption (TPD).[16−18] The $Ni/CeO_2(111)$ surfaces were prepared following the methodology described in detail in refs 16−18. In the experiments of CH_4 activation, the sample was transferred in vacuo to the microreactor at room temperature then the hydrocarbon (1 Torr) was introduced. In the studies investigating the activity of the $Ni/CeO_2(111)$ catalysts for the conversion of methane to methanol, the samples were exposed to a mixture of 1 Torr of CH_4, 0.5 Torr of O_2 and 0−4 Torr of H_2O at room temperature and were rapidly heated to a reaction temperature of 450 K. Product yields (methanol, CO or CO_2) were determined by mass spectroscopy or gas chromatography. In these studies, data were collected in a systematic way at intervals of 5 min. The amount of molecules generated in the catalytic studies was normalized by the total reaction time and the active area exposed by the sample. The kinetic tests were always done in the limit of low conversion (<10%).

The ambient-pressure XPS experiments for the $Ni/CeO_2(111)$ catalysts were performed at the Advanced Light Source in Berkeley, CA (beamline 9.3.2). The XPS spectra were recorded using a VG Scienta R4000 HiPP analyzer. A photon energy of 650 eV was used to excite the O 1s region. The C 1s, Ni 3p, and Ce 4d regions were probed with a photon energy of 490 eV. The total energy resolution in the photoemission experiments was ∼0.2 eV. For the binding energy calibration, we used the Ce 4d photoemission lines and their 122.8 eV satellite features.

Theoretical Models and Computational Methods. We performed spin-polarized density functional theory (DFT) calculations with the DFT+U procedure[19] (an effective onsite Coulomb interaction parameter, U, was applied to the Ce 4*f* states) and the Perdew, Burke, and Ernzerhof (PBE)[20] exchange-correlation functional (GGA). The Vienna ab initio simulation package (VASP)[21] was employed in this study. A value of 4.5 eV[22,23] was used for the Hubbard U-like term. The projector augmented wave method (PAW)[24,25] with a plane-wave cutoff of 415 eV was used. The C (2s, 2p), O (2s, 2p), Ni (3p, 3d, 4s), and Ce (4f, 5s, 5p, 5d, 6s) electrons were treated as valence states. The supported flat Ni_4 cluster on the $CeO_2(111)$ surface was modeled by a (3×3) surface unit cell, with calculated ceria bulk equilibrium lattice constant (CeO_2: 5.485 Å). The ceria surface was modeled employing a nine atomic layer (three O−Ce−O trilayers) slab geometry with at least 12 Å vacuum space. A Monkhorst−Pack grid with $(3 \times 3 \times 1)$ k-points was used. The atoms in the bottom trilayer were kept fixed at their optimized bulk-truncated positions during geometry optimization, whereas the others were allowed to relax. For the O_2, H_2O, CH_4 gas-phase species, Γ-point calculations were performed using a $(12 \times 12 \times 12)$ $Å^3$ box. The climbing image nudged elastic band method (CI-NEB)[26] was employed in order to locate the TS structures. For each reaction pathway, NEBs contained nine images. Only one imaginary frequency was found for each of the TS structures reported in this work.

RESULTS AND DISCUSSION

Figure 1 displays C 1s XPS spectra acquired after exposing clean Ni(111), $CeO_2(111)$ and a $CeO_2(111)$ surface with

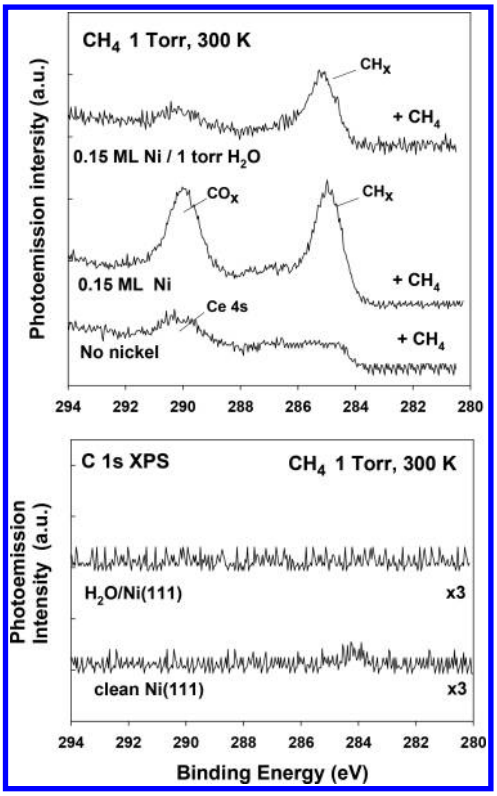

Figure 1. C 1s XPS spectra collected after exposing Ni(111), bottom panel, $CeO_2(111)$ and $Ni/CeO_2(111)$, top panel, to 1 Torr of methane at 300 K for 5 min. To generate the $H_2O/Ni(111)$ and $H_2O/Ni/CeO_2(111)$ samples, the corresponding surfaces were exposed to 1 Torr of water at 300 K before dosing methane.

∼0.15 ML of nickel to 1 Torr of methane at 300 K. Ni(111) is frequently used as a benchmark in experimental and theoretical studies for the activation of methane on metal surfaces.[27−29] On the Ni(111) surface, the C 1s XPS spectrum points to a negligible dissociation of methane in agreement with previous studies which show almost no interaction of the molecule with metal surfaces of pure nickel {(100), (110) and (111) terminations} at room temperature.[27−29] On the pristine $CeO_2(111)$ sample, the adsorption of methane is also negligible. The deposition of small amounts of Ni on a $CeO_2(111)$ film at 300 K produces a partial reduction of the oxide surface and adsorbed NiO_x species (Figure S1 in the Supporting Information).[16,17] In these systems, individual atoms and tiny clusters (2−10 atoms) of nickel are in close contact with the ceria support.[16−18] The electronic perturbations induced by ceria on the nickel have a strong influence on the reactivity of the system toward methane. The top panel in Figure 1 shows a C 1s XPS spectrum recorded after exposing a $CeO_2(111)$ surface containing 0.15 ML of nickel to 1 Torr of CH_4 at room temperature for 5 min. Over the $Ni/CeO_2(111)$ surface, methane is activated and decomposes. Clear peaks are

DOI: 10.1021/jacs.8b03809
J. Am. Chem. Soc. 2018, 140, 7681−7687

seen for CH_x and CO_x groups.[18,30] A significant portion of the reacting methane follows a reaction path which leads to full dissociation: $CH_4 \rightarrow CH_3 \rightarrow CH_2 \rightarrow CH \rightarrow C$. The calculated reaction profile for the dissociation from CH_4 up to CH is shown in Figure 2 over a flat $Ni_4/CeO_2(111)$ model catalysts

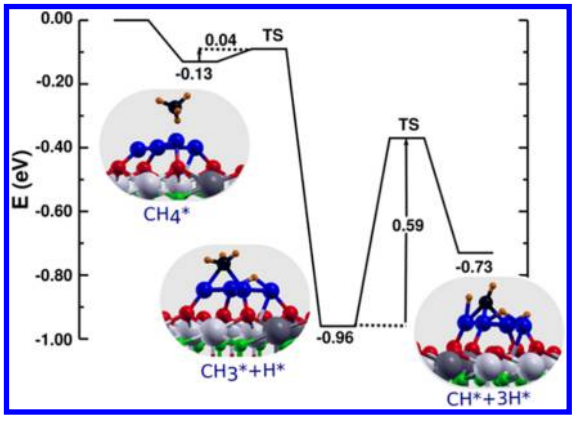

Figure 2. Energy profile for the $CH_4 \rightarrow CH_3$+H → CH + 3H reaction on $Ni_4/CeO_2(111)$. Energies are referenced to the total energy of CH_4(g) and the $Ni_4/CeO_2(111)$ surface. The structures correspond to the side views of the molecularly adsorbed CH_4 and dissociated states. Atom color key: Ni (blue), Ce^{3+} (gray), Ce^{4+} (white), surface/subsurface oxygen atoms (red/green), oxygen atoms from chemisorbed species (red), hydrogen (orange), and carbon atoms (black).

where Ni atoms are oxidized ($Ni^{0.5+}$) and the support is partially reduced (cf. Table S1 and Figure S2),[16] i.e., the computational model matches the essential features of the experimental model catalysts, and there is a clear similarity of the clusters with fragments of Ni(111) terraces. Previous theoretical studies have shown that the binding energy of methane on Ni(111) is negligible (<0.1 eV) with a large activation barrier (0.8−1 eV) for dissociation.[17,31] In contrast, methane reacts with the NiO_x species supported on ceria via the formation of a CH_3 fragment and a H bound to the Ni cluster with a very low activation barrier (0.04 eV). A subsequent dissociation of the methyl species produces directly CH and 2 Ni−H species with a barrier of 0.59 eV, which is surmounted at experimental conditions. Further dissociation produces C adatoms that react with O atoms from the surface to yield CO_x groups.[18] Less than a monolayer of methane reacted with the $Ni/CeO_2(111)$ system at 300 K and there were no significant changes in the oxidation state of Ni and Ce.

Ni(111) interacts poorly with water.[32] After exposing a Ni(111) surface to 1 Torr of water at 300 K, we found a very small amount (<0.1 ML) of oxygen-containing species on the surface, probably produced by the decomposition of the molecule on defect sites.[32] Predosing with water did not enhance the interaction of methane with Ni(111), bottom panel in Figure 1. On a $Ni_4/CeO_2(111)$ substrate, water dissociation, $H_2O \rightarrow OH + H$, is a downhill process (see Figure S3). Experiments of ambient-pressure XPS indicate that H_2O and OH species are coadsorbed on $Ni/CeO_2(111)$ surfaces at 300 K when these systems are in equilibrium with a pressure of gaseous water.[33] However, at higher temperatures (>400 K), only a small amount of OH groups (<0.3 monolayer) is bonded to the $Ni/CeO_2(111)$ surfaces.[33] The ability of $Ni/CeO_2(111)$ to dissociate water[33] can be used to control the reaction selectivity after the activation of CH_4. When H_2O is preadsorbed on $Ni/CeO_2(111)$, the selectivity toward the production of CH_x groups increases to 100% (top spectrum in Figure 1). OH groups probably block surface sites that are highly active for the complete decomposition of methane, formation of $Ni(OH)_2$ is seen in XPS (Figure S1), and the signals for C and CO_x groups vanish from the C 1s data. As we will see below, this phenomenon is essential to push the conversion of methane into methanol.

The CH_x and OH groups coadsorbed on $Ni/CeO_2(111)$ at 300 K do not interact to produce CH_3OH. At this temperature, the system cannot overcome the activation barriers associated with the breaking of HO−surface and H_xC−surface bonds. At a temperature of 450 K, the $Ni/CeO_2(111)$ surface is able to catalyze reactions (1) and (2) but a significant production of methanol was seen only in the presence of water. Figure 3

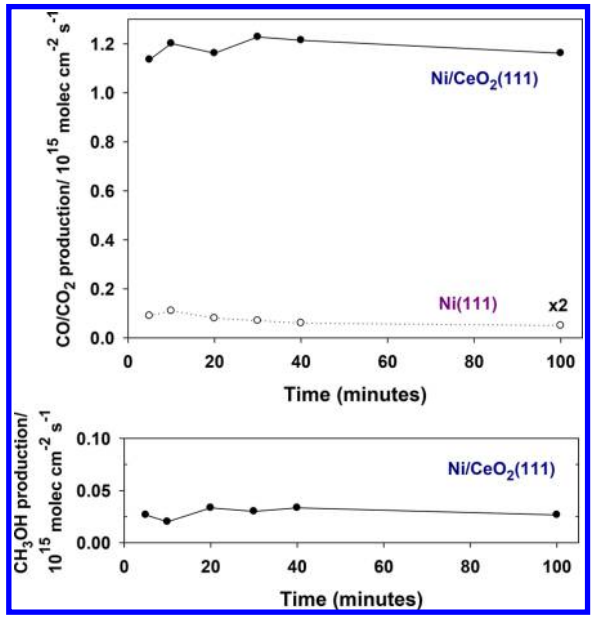

Figure 3. Production of CO/CO_2, top panel, and methanol, bottom panel, on Ni(111) and $Ni/CeO_2(111)$ catalysts as a function of time. The Ni coverage on ceria was ~0.15 ML. The sample was exposed to 1 Torr of CH_4 and 0.5 Torr of O_2 at 450 K. No methanol production was detected over the Ni(111) catalyst.

compares the rates for the reactions on Ni(111) and $Ni/CeO_2(111)$ surfaces as a function of time with a mixture of CH_4 and O_2 in the feed. Ni(111) displays a very low activity for the combustion of methane to CO/CO_2 and we did not detect the formation of any methanol on this catalyst. No activity for reactions (1) and (2) was found on plain $CeO_2(111)$ under the reaction conditions used for the experiments in Figure 3. In the case of 0.15 ML of Ni on $CeO_2(111)$, we found a very good active and stable catalyst for the combustion of methane with the formation of some methanol. Without water in the reaction feed, the production of methanol is very small and CO/CO_2 and H_2 are the main reaction products. The highly active surface sites are not covered by OH species and thus the $CH_4 + nO_2 \rightarrow CO/CO_2 + H_2$ reaction occurs instead of CH_3OH formation. Since both reaction pathways are possible from a thermodynamic viewpoint,[2] most of the CH_3OH generated may be decomposed into CO/CO_2.[3−6] However, in a water rich environment the catalytic production of methanol increases significantly as shown in Figure 4. At a 4:1 ratio of H_2O:CH_4, the selectivity toward methanol formation was ~35%. A higher H_2O:CH_4 ratio did not improve the selectivity

DOI: 10.1021/jacs.8b03809
J. Am. Chem. Soc. 2018, 140, 7681−7687

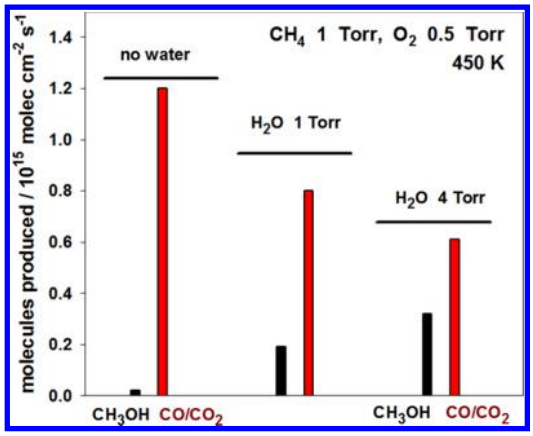

Figure 4. Production of methanol on a $Ni/CeO_2(111)$ catalyst as a function of water pressure. The Ni coverage on ceria was ~0.15 ML. The sample was exposed to 1 Torr of CH_4, 0.5 Torr of O_2, and 0, 1, or 4 Torr of H_2O at 450 K.

for methanol formation and substantially decreased the conversion of methane. OH groups formed by the dissociation of water on the $Ni/CeO_2(111)$ surface[33] probably blocked sites necessary for the bonding and activation of methane. The best selectivity toward methanol production observed in this study is larger than the best selectivity reported in the literature for ceria- and zirconia-based powder catalysts which contain NiO as an active phase.[34]

The results in Figure 3 point to strong effects of metal–support interactions on the catalytic process. Formation of methanol was seen only when a nickel–ceria interface existed and the $Ni/CeO_2(111)$ catalyst was much more active for the conversion of methane than Ni(111). A plot of the catalytic activity for the production of methanol on $Ni/CeO_2(111)$ as a function of nickel coverage, Figure 5, also reflects the effects of a strong metal–support interaction. For small coverages of Ni on ceria (<0.2 ML), results of valence and core-level photoemission show that the oxide induces strong electronic perturbations on nickel.[35] These electronic perturbations decrease at higher Ni coverages and the catalytic activity for

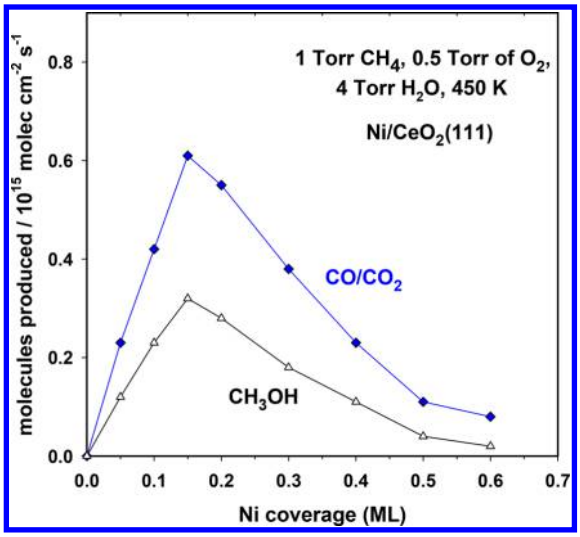

Figure 5. Production of CO/CO_2 and CH_3OH on $Ni/CeO_2(111)$ catalysts as a function of nickel coverage. The samples were exposed to 1 Torr of CH_4, 0.5 Torr of O_2, and 4 Torr of H_2O at 450 K.

the production of CO/CO_2 and CH_3OH drops. The catalysts with nickel coverages below 0.3 ML did not show any signs for deactivation after performing the reaction for 100 min maintaining their activity and selectivity; they did survive several catalytic cycles at a temperature of 450 K.

Using ambient-pressure X-ray photoelectron spectroscopy (AP-XPS), we investigated the surface chemistry associated with the activation and conversion of methane on $Ni/CeO_2(111)$. Figure 6 shows C 1s XPS spectra collected while

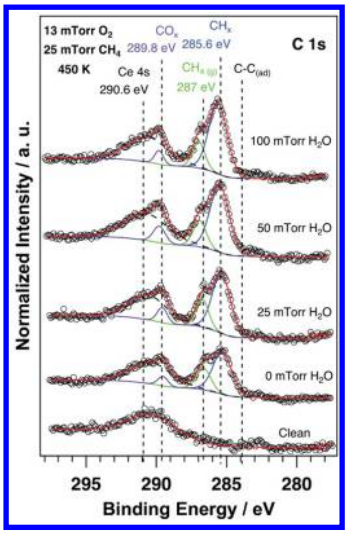

Figure 6. C 1s XPS spectra acquired while exposing a $CeO_2(111)$ surface precovered with 0.15 ML of nickel to a reaction mixture of methane (25 mTorr) and O_2 (13 mTorr) without and with water (0, 25, 50, 100 m Torr). The temperature of the sample was 450 K.

exposing a low-loaded $Ni/CeO_2(111)$ catalyst to a mixture of CH_4/O_2 with and without water. As the pressure of water in the background increases, there is an increase in the signal for adsorbed CH_x groups that can be transformed into methanol with the amount of surface CO_x present always being small. In the C 1s region, we did not see any signal that could be attributed to adsorbed CH_3O or CH_3OH. Thus, at 450 K, the $CH_3 \rightarrow CH_3O \rightarrow CH_3OH$ conversion probably occurs very fast when water is present in the reaction mixture. In principle, the oxygen atom present in methanol could be coming from adsorbed O atoms or OH groups which are present on the surface (Figure S4).

Figure 7 displays Ce 4d and Ni 3p XPS spectra collected together with the experiments shown in Figure 6. In Figure 7A, one sees the characteristic line-shape and features for CeO_2.[17] We found that the hydrogen produced by the dissociation of pure methane at high temperature could reduce the ceria substrate,[34] but in the presence of oxidizing agents (O_2, H_2O), a reduction process is impossible. This is good because Ce^{3+} sites present in ceria could decompose the formed methanol.[36] In Figure 7B, the Ni 3p features exhibit a line-shape that could be a product of the existence of Ni^{2+} species, such as $Ni(OH)_2$ and NiO. The dosing of H_2O to $Ni/CeO_2(111)$ at room temperature (Figure S1) produces $Ni(OH)_2$ as a dominant species, but at 473 K and under a reaction mixture that also contains CH_4 and O_2, the relative concentration of the nickel hydroxide decreases. A large fraction of the OH groups seen in AP-XPS (Figure S1) is probably bound to ceria sites. In the catalysts, Ni could dissociate CH_4, water and O_2 (which, for our $Ni_4/CeO_2(111)$ theoretical model catalyst, was also considered,

DOI: 10.1021/jacs.8b03809
J. Am. Chem. Soc. 2018, 140, 7681–7687

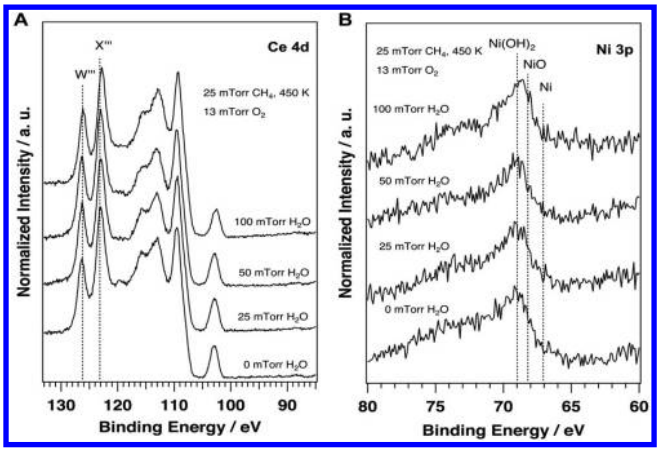

Figure 7. Ce 4d and Ni 3p XPS spectra acquired while exposing a $CeO_2(111)$ surface precovered with 0.15 ML of nickel to a reaction mixture of methane (25 mTorr) and O_2 (13 mTorr) without and with water (0, 25, 50, 100 m Torr). The temperature of the sample was 450 K.

see Figures 2, S3, and S5), and ceria probably dissociates O_2 and water at Ce^{3+} sites produced by the Ni deposition. The material was active and stable as a catalyst for the production of methanol only when methane, O_2 and water were present in the feed. A feed with only methane and O_2 produced a negligible amount of methanol. For a feed with methane and water, we found a slow reduction of the system and eventual deactivation by carbon deposition. In the absence of O_2, the oxidizing capacity of water was not able to balance the reducing power of methane.

To obtain microscopic insight into possible reaction paths and the special role of water into the behavior of the low-loaded Ni-$CeO_2(111)$ system for the production of methanol from methane and oxygen, we studied the process by using calculations based on a spin-polarized density functional theory (DFT+U) approach. We modeled the experimental Ni-CeO_2 system using small flat Ni_4 clusters on a $CeO_2(111)$ surface.[16] These Ni_4 species partially reduce the support, with the formation of two Ce^{3+}, i.e., the Ni atoms in direct contact with the reducible ceria support are partially oxidized (cf. Table S1).

As mentioned above, molecular oxygen readily dissociates to chemisorbed atomic species on the ceria-supported Ni_4 species (cf. Figure S5). Thus, we considered a partially oxygen covered $Ni_4/CeO_2(111)$ system to calculate the CH_4 to CH_3OH reaction profile (Figure 8). The molecular binding of CH_4 to the oxidized Ni_4 particles is not that strong (0.14 eV; structure II) with an activation barrier for the first hydrogen abstraction of 0.54 eV (TS_1, Figure 8). This is somewhat larger than that for the $Ni_4/CeO_2(111)$ system without chemisorbed oxygen, but is comparable to that for the further decomposition of the methyl species on that system (cf. Figure 2). After the activation of methane on the $O/Ni_4/CeO_2(111)$ surface, methoxy species could form, but the activation barrier would be large, 1.16 eV (TS_{a1}, Figure 8). Instead, the methyl species would dissociate ($CH_3 \rightarrow CH_2 + H$) with a smaller barrier of 1.01 eV (TS_{a2}, Figure 8).

The addition of water, however, changes the reaction path. The adsorbed water molecule (structure IV) dissociates by overcoming a relatively low-energy activation barrier (TS_2 = 0.31 eV, Figure 8), producing a surface hydroxyl group (O_sH) on the ceria support (accompanied by the formation of an additional Ce^{3+}), whereas the water OH group recombines with the hydrogen previously abstracted from methane, forming a new adsorbed water molecule (structure V). Once more, methoxy species could form, but the activation barrier would also be large, 1.27 eV (TS_{b1}, Figure 8). Instead, the methyl species would dissociate with a smaller barrier of 0.76 eV (TS_{b2},

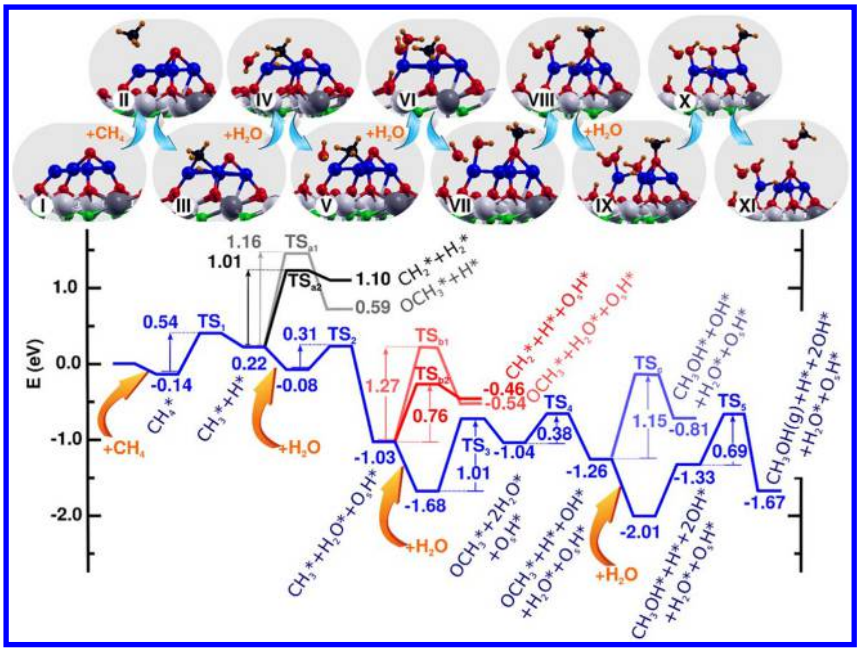

Figure 8. Energy profile for the CH_4 to CH_3OH reaction over an $O/Ni_4/CeO_2(111)$ surface under the presence of H_2O. Energies are referenced to the total energy of CH_4 (g), $3H_2O$ (g) and the $Ni_4/CeO_2(111)$ surface with chemisorbed oxygen. The side views of the optimized structures are included. Atom color key: Ni (blue), Ce^{3+} (gray), Ce^{4+} (white), surface/subsurface lattice oxygen atoms (red/green), oxygen atoms from chemisorbed species (red), hydrogen (orange), and carbon atoms (black). The principal reaction path is depicted in blue, whereas alternative routes are shown in black, gray, red and light red, as well as light blue.

DOI: 10.1021/jacs.8b03809
J. Am. Chem. Soc. 2018, 140, 7681−7687

Figure 8). Thus, more water is added to the system (structure VI). At this point, there is enough chemisorbed water to block all Ni sites necessary for methyl species to dissociate relatively easily (cf. Figure S6) and thus a methoxy species forms on nickel (structure VII) via a 1.01 eV transition state (TS_3, Figure 8).

Further dissociation of a chemisorbed water species stabilizes the system yielding chemisorbed H and OH species on the nickel cluster (structure VII). The activation energy for the formation of CH_3OH from the chemisorbed OCH_3 and H species is calculated to be 1.15 eV (TS_c, Figure 8), comparable with the methoxy formation barrier. However, if additional water is adsorbed (structure IX), it could donate one H to the methoxy species and thus form CH_3OH without a barrier (structure X). The desorption of methanol occurs via a 0.69 eV transition state (TS_5, Figure 8) which is accompanied by the adsorption of a OH species at the catalyst site from which CH_3OH has desorbed.

In the present study, we used ambient pressure X-ray photoelectron spectroscopy and performed DFT+U calculations to elucidate the reaction mechanism for the direct CH_4 conversion to CH_3OH at the surface of a low-loaded Ni-CeO_2 catalyst. This system exhibits features not seen in catalysts able to perform a $CH_4 \rightarrow CH_3OH$ transformation such as copper-exchanged zeolites[6,12] or a model inverse oxide/metal catalyst like CeO_2/CuO_x/Cu(111).[14] On one hand, we show that the reducible ceria support modifies the electronic properties of the nickel in direct contact with it, changing its oxidation state while becoming oxidized. This, in turn, results in chemical properties which are very different from those of the corresponding larger three-dimensional nanoparticles or extended nickel surfaces. These metal−support interactions play an essential role in the easy cleavage of O−H and C−H bonds, which is crucial for the dissociation of H_2O as well as the activation of CH_4 which is needed in the CH_4 conversion to CH_3OH with O_2 present in the feed. Note that, contrary to large three-dimensional Ni nanoparticles, the presence of Ni adatoms, which are oxidized (Ni^{2+}), is not detrimental to the activity since O−H and C−H bonds can be easily cleaved over them.[17,33] The metal−support interactions seen in our catalysts lead to a much better selectivity toward methanol production than that observed in other types of ceria- and zirconia-based catalysts.[34] On the other hand, we show that water in excess is absolutely necessary for avoiding the complete decomposition of methane on the partially oxidized Ni nanoparticles, which would yield CO and/or CO_2. The role of water is twofold. First, it blocks Ni active sites by dissociating over them, yielding chemisorbed OH and H species. As a consequence, CH_3 would rather form OCH_3 species with existing chemisorbed O species than further decompose. Second, water also helps the formation and desorption of CH_3OH. Water provides a H atom and a OH species for the $Ni-OCH_3 + Ni-H \rightarrow Ni-OH + Ni + CH_3OH(g)$ reaction to occur. On the Ni/CeO_2 surfaces, one sees a reaction mechanism for the direct $CH_4 \rightarrow CH_3OH$ conversion not seen over copper-exchanged zeolites[6,12] or model inverse oxide/metal catalyst like CeO_2/CuO_x/Cu-(111).[14]

CONCLUSION

Metal−support interactions and water site-blocking play a crucial role in the conversion of methane to methanol on Ni/CeO_2 catalysts. The metal−support interactions make possible the binding and activation of water and methane at low temperature while the water site-blocking tunes the surface reactivity and enhances the selectivity toward methanol formation. A survey of the literature shows that water also plays an essential role in the stepwise formation of methanol from methane on copper-exchanged zeolites[3,6] and also for the direct catalytic conversion over a model inverse CeO_2/CuO_x/Cu(111) catalyst[14] but the interplay between CH_3 species, O adatoms, and water molecules is different on a Ni/ceria catalyst. Although water-site blocking is important, one still needs the effects of metal−support interactions to bind and activate methane and water. We believe that the conceptual ideas presented here can be quite useful for the design of other conventional metal/oxide catalysts which can achieve the transformation of methane to methanol.

ASSOCIATED CONTENT

Supporting Information

The Supporting Information is available free of charge on the ACS Publications website at DOI: 10.1021/jacs.8b03809.

XPS spectra, structural $Ni_4/CeO_2(111)$ model, and Bader charges as well as reaction profiles calculated with DFT; geometries of all the stationary points and transition state structures whose relative energies are given in the article, along with their calculated total energies and imaginary frequencies (PDF)

AUTHOR INFORMATION

Corresponding Authors

*vgp@icp.csic.es
*ssenanay@bnl.gov
*rodrigez@bnl.gov

ORCID

Zongyuan Liu: 0000-0001-8526-5590
M. Verónica Ganduglia-Pirovano: 0000-0003-2408-8898
Sanjaya D. Senanayake: 0000-0003-3991-4232
José A. Rodriguez: 0000-0002-5680-4214

Notes

The authors declare no competing financial interest.

ACKNOWLEDGMENTS

The work carried out at Brookhaven National Laboratory was supported by the U.S. Department of Energy (Chemical Sciences Division, DE-SC0012704). S.D.S. is supported by a U.S. Department of Energy Early Career Award. This research used resources of the Advanced Light Source (Beamline 9.3.2), which is a DOE Office of Science User Facility under contract no. DE-AC02-05CH11231. Authors acknowledge contribution of Dr. Ethan Crumlin for assistance with AP-XPS measurements. M.V.G.-P. acknowledges the financial support of the Ministry of Economy and Competitiveness MINECO-Spain (Grant No. CTQ2015-78823-R) and P.G.L. that of the Agencia Nacional de Promoción Científica y Tecnológica-Argentina (Grant No. PICT-2016-2750). Computer time provided by the BIFI-ZCAM, RES at the Marenostrum and LaPalma nodes, SNCAD (Sistema Nacional de Computación de Alto Desempeño, Argentina), and the DECI resources BEM based in Poland at WCSS and Archer at EPCC with support from the PRACE aislb, is acknowledged. M.V. thanks the Ministry of Education, Youth and Sports of the Czech Republic for financial support under Project LH15277. R.M.P. was partially funded by the AGEP-T (Alliance for Graduate Education and

DOI: 10.1021/jacs.8b03809
J. Am. Chem. Soc. 2018, 140, 7681−7687

the Professoriate−Transformation) which is funded by the National Science Foundation, award #1311318.

REFERENCES

(1) *Methane in the Environment: Occurence, Uses and Pollution*; Basile, A., Ed.; Nova Science Publication Inc, 2013.
(2) Khirsariya, P.; Mewada, R. K. *Procedia Eng.* **2013**, *51*, 409−415.
(3) Grundner, S.; Markovits, M. A. C.; Li, G.; Tromp, M.; Pidko, E. A.; Hensen, E. J. M.; Jentys, A.; Sanchez-Sanchez, M.; Lercher, J. A. *Nat. Commun.* **2015**, *6*, 7546−7555.
(4) Li, G.; Vassilev, P.; Sanchez-Sanchez, M.; Lercher, J. A.; Hensen, E. J. M.; Pidko, E. A. *J. Catal.* **2016**, *338*, 305−312.
(5) Tomkins, P.; Ranocchiari, M.; van Bokhoven, J. A. *Acc. Chem. Res.* **2017**, *50*, 418−425.
(6) Sushkevich, V. L.; Palagin, D.; Ranocchiari, M.; van Bokhoven, J. A. *Science* **2017**, *356*, 523−527.
(7) Chan, S. I.; Yu, S.S.-F. *Acc. Chem. Res.* **2008**, *41*, 969−979.
(8) Chan, S. I.; Lu, Y.-J.; Nagababu, P.; Maji, S.; Hung, M. C.; Lee, M. M.; Hsu, I.-J.; Minh, P. D.; Lai, J.C.-H.; Ng, K. Y.; Ramalingam, S.; Yu, S.S.-F.; Chan, M. K. *Angew. Chem., Int. Ed.* **2013**, *52*, 3731−3735.
(9) Xu, J.; Zheng, A.; Wang, X.; Qi, G.; Su, J.; Du, J.; Gan, Z.; Wu, J.; Wang, W.; Deng, F. *Chem. Sci.* **2012**, *3*, 2932−2940.
(10) Olivos-Suarez, A. I.; Szécsényi, A.; Hensen, E. J. M.; Ruiz-Martinez, J.; Pidko, E. A.; Gascon, J. *ACS Catal.* **2016**, *6*, 2965−2981.
(11) Chin, Y.-H.; Buda, C.; Neurock, M.; Iglesia, E. *J. Am. Chem. Soc.* **2013**, *135*, 15425−15442.
(12) Narsimhan, K.; Iyoki, K.; Dinh, K.; Román-Leshkov, Y. *ACS Cent. Sci.* **2016**, *2*, 424−429.
(13) Ravi, M.; Ranocchiari, M.; van Bokhoven, J. A. *Angew. Chem., Int. Ed.* **2017**, *56*, 16464−16483.
(14) Zuo, Z.; Ramírez, P. J.; Senanayake, S. D.; Liu, P.; Rodriguez, J. A. *J. Am. Chem. Soc.* **2016**, *138*, 13810−13813.
(15) Pappas, D. K.; Borfecchia, E.; Dyballa, M.; Pankin, I. A.; Lomachenko, K. A.; Martini, A.; Signorile, M.; Teketel, S.; Arstad, B.; Berlier, G.; Lamberti, C.; Bordiga, S.; Olsbye, U.; Lillerud, K. P.; Svelle, S.; Beato, P. *J. Am. Chem. Soc.* **2017**, *139*, 14961−14975.
(16) Carrasco, J.; Barrio, L.; Liu, P.; Rodriguez, J. A.; Ganduglia-Pirovano, M. V. *J. Phys. Chem. C* **2013**, *117*, 8241−8250.
(17) Lustemberg, P. G.; Ramírez, P. J.; Liu, Z.; Gutiérrez, R. A.; Grinter, D. G.; Carrasco, J.; Senanayake, S. D.; Rodriguez, J. A.; Ganduglia-Pirovano, M. V. *ACS Catal.* **2016**, *6*, 8184−8191.
(18) Liu, Z.; Grinter, D. G.; Lustemberg, P. G.; Nguyen-Phan, T.-D.; Zhou, Y.; Luo, S.; Waluyo, I.; Crumlin, E. J.; Stacchiola, D. J.; Zhou, J.; Carrasco, J.; Busnengo, H. F.; Ganduglia-Pirovano, M. V.; Senanayake, S. D.; Rodriguez, J. A. *Angew. Chem., Int. Ed.* **2016**, *55*, 7455−7459.
(19) Dudarev, S.; Botton, G.; Savrasov, S.; Humphreys, C.; Sutton, A. *Phys. Rev. B: Condens. Matter Mater. Phys.* **1998**, *57*, 1505−1509.
(20) Perdew, J. P.; Burke, K.; Ernzerhof, M. *Phys. Rev. Lett.* **1996**, *77*, 3865−3868.
(21) http://www.vasp.at; version vasp.5.3.5.
(22) Fabris, S.; Vicario, G.; Balducci, G.; de Gironcoli, S.; Baroni, S. *J. Phys. Chem. B* **2005**, *109*, 22860−22867.
(23) Cococcioni, M.; de Gironcoli, S. *Phys. Rev. B: Condens. Matter Mater. Phys.* **2005**, *71*, 35105−35120.
(24) Kresse, G.; Joubert, D. *Phys. Rev. B: Condens. Matter Mater. Phys.* **1999**, *59*, 1758−1775.
(25) Blöchl, P. E. *Phys. Rev. B: Condens. Matter Mater. Phys.* **1994**, *50*, 17953−17979.
(26) Henkelman, G.; Uberuaga, B. P.; Jónsson, H. *J. Chem. Phys.* **2000**, *113*, 9901−9904.
(27) Beebe, T. P., Jr.; Goodman, D. W.; Kay, B. D.; Yates, J. T. *J. Chem. Phys.* **1987**, *87*, 2305−2315.
(28) Campbell, R. A.; Szanyi, J.; Lenz, P.; Goodman, D. W. *Catal. Lett.* **1993**, *17*, 39−46.
(29) Yuan, K.; Zhong, J.-Q.; Zhou, X.; Xu, L.; Bergman, S. L.; Wu, K.; Xu, G. Q.; Bernasek, S. L.; Li, H. X.; Chen, W. *ACS Catal.* **2016**, *6* (7), 4330−4339.
(30) Liu, Z.; Duchoň, T.; Wang, H.; Peterson, E. W.; Zhou, Y.; Luo, S.; Zhou, J.; Matolín, V.; Stacchiola, D. J.; Rodriguez, J. A.; Senanayake, S. D. *J. Phys. Chem. C* **2015**, *119*, 18248−18256.
(31) Zhou, X.; Nattino, F.; Zhang, Y.; Chen, J.; Kroes, G.-J.; Guo, H.; Jiang, B. *Phys. Chem. Chem. Phys.* **2017**, *19*, 30540−30550.
(32) Zhao, W.; Carey, S. J.; Mao, Z.; Campbell, C. T. *ACS Catal.* **2018**, *8*, 1485−1489.
(33) Carrasco, J.; López-Durán, D.; Liu, Z.; Duchoň, T.; Evans, J.; Senanayake, S. D.; Crumlin, E. J.; Matolín, V.; Rodriguez, J. A.; Ganduglia-Pirovano, M. V. *Angew. Chem., Int. Ed.* **2015**, *54*, 3917−3921.
(34) Okolie, C.; Belhseine, Y. F.; Lyu, Y.; Yung, M. M.; Engelhard, M. H.; Kovarik, L.; Stavitski, E.; Sievers, C. *Angew. Chem., Int. Ed.* **2017**, *56*, 13876−13881.
(35) Senanayake, S.; Evans, J.; Agnoli, S.; Barrio, L.; Chen, T.-L.; Hrbek, J.; Rodriguez, J. A. *Top. Catal.* **2011**, *54*, 34−41.
(36) Albrecht, P. M.; Mullins, D. R. *Langmuir* **2013**, *29*, 4559−4567.

DOI: 10.1021/jacs.8b03809
J. Am. Chem. Soc. 2018, 140, 7681−7687